Nucleon axial form factors from lattice QCD

Constantia Alexandrou[1⋆]

Department of Physics, University of Cyprus, PO Box 20537, 1678 Nicosia, Cyprus, and
Computation-based Science and Technology Research Center, The Cyprus Institute, 20, Constantinou Kavafi Str., Nicosia 2121, Cyprus
*alexand@ucy.ac.cy

January 26, 2022

XXXIII International (ONLINE) Workshop on High Energy Physics
"Hard Problems of Hadron Physics: Non-Perturbative QCD & Related Quests"
November 8-12, 2021
doi:10.21468/SciPostPhysProc.?

Abstract

We give an overview on the evaluation of the axial and pseudoscalar form factors of the nucleon within the lattice QCD formulation. We discuss recent results obtained from the analysis of $N_f = 2+1+1$ twisted mass fermion gauge ensembles generated at physical values of the pion mass. Besides evaluating the isovector form factors, and the PCAC and Goldberger-Treiman relations, we also discuss results for the strange and charm axial form factors. We provide a comparison with other recent lattice QCD results obtained with different discretization schemes of the fermion action.

Contents

---

1 Introduction

The electromagnetic form factors of the nucleon have been extensively studied experimentally for many years leading to their precise determination, for recent results see e.g. [1, 2]. Thus, they are being used to benchmark theoretical approaches. However, the nucleon axial form factors are less well known. The axial form factors are important quantities needed for studying weak interaction processes both theoretically and experimentally. The nucleon matrix element of the isovector axial-vector current A_μ can be expressed in terms of two form factors, the axial, $G_A(Q^2)$, and the induced pseudoscalar $G_P(Q^2)$. The axial form factor, $G_A(Q^2)$, is experimentally determined from elastic scattering of neutrinos with protons, $\nu_\mu + p \to \mu^+ + n$ [3,4], while $G_P(Q^2)$ from the longitudinal cross section in pion electro-production [5]. The axial charge $g_A \equiv G_A(0)$ can be measured in high precision from β-decay experiments [6, 7]. The induced pseudoscalar coupling g_P^* can be determined via the muon capture process $\mu^- + p \to n + \nu_\mu$ at momentum transfer squared of $Q^2 = 0.88 m_\mu^2$ [8, 9], where m_μ is the muon mass. If one computes also the pseudoscalar form factor $G_P(Q^2)$ one can check important phenomenological relations, such as the partially conserved axial-vector current (PCAC) relation. Furthermore, at low momentum transfer square Q^2 and assuming pion pole dominance (PPD), one can relate $G_A(Q^2)$ to $G_P(Q^2)$ and derive the Goldberger-Treiman (GT) relation.

Beyond isovector axial form factors mentioned above, it is also interesting to study the isoscalar, strange and charm quark axial form factors. There is a rich experimental program studying parity-violating processes asymmetries. Results in forward elastic electron-proton scattering by HAPPEX [10] combined with data from neutrino and antineutrino-proton elastic scattering cross sections from Brookhaven E734 [11] determined both the strange vector and axial form factors of the proton at non-zero Q^2 [12]. Additional parity-violating data from the G0 experiments [13, 14] improved the determination of the strange axial form factors and the MicroBooNE neutrino detector at FermiLab aims ar extracting it for $Q^2 \in 1 - 0.08$ GeV^2 . To date, the axial form factors are the main source of error in the description of neutrino-nucleon interactions. Therefore, a calculation of these form factors from first principle is important and will provide valuable input to phenomenology and to on-going and future experiments, such as DUNE [15] and Hyper-K [16].

Lattice Quantum Dynamics (QCD) provides the *ab initio* non-perturbative framework for computing from factors using directly the QCD Lagrangian. Early studies of the nucleon axial form factors were done using dynamical fermion simulations at heavier than physical pion masses, as e.g. in Ref. [17]. Only recently, several groups are computing the axial form factors using simulations generated directly at the physical value of the pion mass [18–24]. The results discussed here are mostly based on Refs. [25, 26].

2 Isovector axial and pseudoscalar form factors and their relations

On the hadron level, the nucleon matrix element of the isovector axial-vector current, $A_\mu = \bar{u}\gamma_\mu\gamma_5 u - \bar{d}\gamma_\mu\gamma_5 d$, is decomposed into two Lorenz-invariant isovector form factors, the axial form factor $G_A(Q^2)$, and the induced pseudoscalar, $G_P(Q^2)$:

$$\langle N(p',s')|A_\mu|N(p,s)\rangle = \bar{u}_N(p',s')\left[\gamma_\mu G_A(Q^2) - \frac{Q_\mu}{2m_N} G_P(Q^2)\right]\gamma_5 u_N(p,s), \tag{1}$$

where u_N is the nucleon spinor with initial (final) momentum $p(p')$ and spin $s(s')$, $q = p' - p$ the momentum transfer and $q^2 = -Q^2$. The nucleon pseudoscalar matrix element is parameterized in terms of a single form factor $G_5(Q^2)$ as

$$\langle N(p',s')|P_5|N(p,s)\rangle = G_5(Q^2)\bar{u}_N(p',s')\gamma_5 u_N(p,s), \tag{2}$$

where $P_5 = \bar{u}\gamma_5 u - \bar{d}\gamma_5 d$. We omit the superscripts on isovector quantities, unless otherwise indicated. Isoscalar, strange and charm quantities have a corresponding superscript.

At the form factors level partial conservation of the axial-vector current (PCAC) relates $G_A(Q^2)$ and $G_P(Q^2)$ to $G_5(Q^2)$ as follows

$$G_A(Q^2) - \frac{Q^2}{4m_N^2} G_P(Q^2) = \frac{m_q}{m_N} G_5(Q^2). \tag{3}$$

Expressing the pion field as $\psi_\pi = \frac{2m_q P}{F_\pi m_\pi^2}$, one can connect $G_P(Q^2)$ to the pion-nucleon form factor $G_{\pi NN}(Q^2)$ as

$$G_5(Q^2) = \frac{F_\pi m_\pi^2}{m_q} \frac{G_{\pi NN}(Q^2)}{m_\pi^2 + Q^2}. \tag{4}$$

Eq. (4) is written so that it illustrates the pole structure of $G_5(Q^2)$. Substituting $G_5(Q^2)$ in Eq. (3), one obtains the GT relation [17, 27]

$$G_A(Q^2) - \frac{Q^2}{4m_N^2} G_P(Q^2) = \frac{1}{m_N} \frac{G_{\pi NN}(Q^2) F_\pi m_\pi^2}{m_\pi^2 + Q^2}. \tag{5}$$

The pion-nucleon form factor $G_{\pi NN}(Q^2)$ at the pion pole gives the pion-nucleon coupling $g_{\pi NN} \equiv G_{\pi NN}(Q^2 = -m_\pi^2)$. In the limit $Q^2 \to -m_\pi^2$, the pole on the right hand side of Eq. (5) must be compensated by a similar one in $G_P(Q^2)$, since $G_A(-m_\pi^2)$ is finite. Therefore, if we multiply Eq. (5) by $(Q^2 + m_\pi^2)$ we have

$$\lim_{Q^2 \to -m_\pi^2} (Q^2 + m_\pi^2) G_P(Q^2) = 4 m_N F_\pi g_{\pi NN} \tag{6}$$

and, thus, one can extract $g_{\pi NN}$ from $G_P(Q62)$. Assuming pion pole dominance and for $\lim_{Q^2 \to -m_\pi^2}$, $G_P(Q^2) = 4m_N F_\pi G_{\pi NN}(Q^2)/(m_\pi^2 + Q^2)$. Inserting this expression for $G_P(Q^2)$ in Eq. (5) we obtain the GT relation [28]

$$m_N G_A(Q^2) = F_\pi G_{\pi NN}(Q^2), \tag{7}$$

which means that $G_P(Q^2)$ can be expressed as [29]

$$G_P(Q^2) = \frac{4m_N^2}{Q^2 + m_\pi^2} G_A(Q^2). \tag{8}$$

From Eq. (7), the pion-nucleon coupling can be expressed as $g_{\pi NN} = m_N G_A(-m_\pi^2)/F_\pi$. In the chiral limit, $\lim_{m_\pi \to 0} G_A(-m_\pi^2) \to g_A$ and we have that $g_{\pi NN} = \frac{m_N}{F_\pi} g_A$, which at finite pion mass receives corrections. The deviation from equality is known as the GT discrepancy given by $\Delta_{GT} \equiv 1 - \frac{g_A m_N}{g_{\pi NN} F_\pi}$ and it is estimated to be at the 2% level [30].

3 Determination of nucleon matrix in lattice QCD

In order to extract the nucleon matrix elements one need to calculate the appropriate three-point functions, as schematically shown in Fig. 1. The three-point function is given by

$$C_\mu(\Gamma_k, \vec{q}, \vec{p}\,'; t_s, t_{\rm ins}, t_0) = \sum_{\vec{x}_{\rm ins}, \vec{x}_s} e^{i(\vec{x}_{\rm ins} - \vec{x}_0)\cdot\vec{q}} e^{-i(\vec{x}_s - \vec{x}_0)\cdot\vec{p}\,'} \times {\rm Tr}\left[\Gamma_k \langle \mathcal{J}_N(t_s, \vec{x}_s) A_\mu(t_{\rm ins}, \vec{x}_{\rm ins}) \bar{\mathcal{J}}_N(t_0, \vec{x}_0)\rangle\right], \tag{9}$$

where $\Gamma_k = i\Gamma_0\gamma_5\gamma_k$ and $\bar{\mathcal{J}}_N$ creates states with the quantum numbers of the nucleon. From now on we will use $\vec{p}\,' = \vec{0}$.

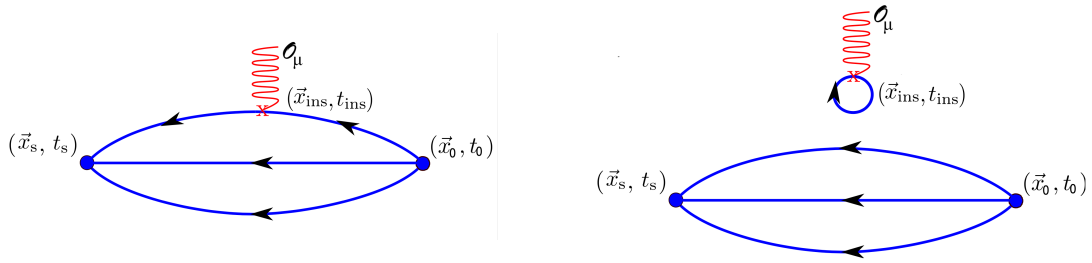

Figure 1: Diagrammatic representation of three-point functions (left: connected, right: disconnected) needed for the determination of nucleon matrix elements. $\mathcal{O}_\mu$ is the operator whose nucleon matrix element we seek to evaluate e.g. the axial vector current A_μ.

The Euclidean time dependence of the three-point function and unknown overlaps of the interpolating field with the nucleon state, are canceled in an appropriately constructed ratio of three- to a combination of two-point functions [31–34],

$$R_\mu(\Gamma_k, \vec{q}; t_s, t_{\rm ins}) = \frac{C_\mu(\Gamma_k, \vec{q}; t_s, t_{\rm ins}\ )}{C(\Gamma_0, \vec{0}; t_s)} \times \sqrt{\frac{C(\Gamma_0, \vec{q}; t_s - t_{\rm ins})C(\Gamma_0, \vec{0}; t_{\rm ins})C(\Gamma_0, \vec{0}; t_s)}{C\ (\Gamma_0, \vec{0}; t_s - t_{\rm ins})C(\Gamma_0, \vec{q}; t_{\rm ins})C(\Gamma_0, \vec{q}; t_s)}}, \tag{10}$$

where we take t_s and $t_{\rm ins}$ relative to the source time t_0, or equivalently t_0 is set to zero. In the limit of large time separations $(t_s - t_{\rm ins}) \gg a$ and $t_{\rm ins} \gg a$, the ratio in Eq. (10 converges to the nucleon ground state matrix element, namely

$$R_\mu(\Gamma_k; \vec{q}; t_s; t_{\rm ins}) \xrightarrow[t_{\rm ins} \gg a]{t_s - t_{\rm ins} \gg a} \Pi_\mu(\Gamma_k; \vec{q})\,. \tag{11}$$

Three well-established methods are used to identify ground state dominance, namely the *plateau, summation* and *two-state fit* methods [25]. In the two-state fit we consider contributions from both the ground and first excited states. We allow the first excited state in the three-point function to be in general different from that of the two-point function. The reason is that multi-particle states are volume suppressed and are typically not observed in the two-point function. However, if they couple strongly to a current they may contribute in the three-point function. As pointed out in Refs. [35, 36], this may happen for the case of the axial-vector current considered here. In order investigate the possibility that multi-particle states contribute to the three-point function, we perform the following two types of fits:

M1: We assume that the first excited state is the same in both the two- and three-point functions and first fit the two-point function to extract the first excited energy $E_1(\vec{p})$ and overlap factor. We then input this information into our fit of the ratio of Eq. (10). We also fit the zero momentum two-point function to determine the nucleon mass and then use the continuum dispersion relation $E_0(\vec{p}) = \sqrt{m_N^2 + \vec{p}^{\,2}}$ to determine the nucleon energy for a given value of momentum. The continuum dispersion relation is satisfied for all the momenta considered. We will refer to this as fit *M1*.

M2: We allow the first excited state to be different in the two- and three- point functions. In this case, the first excited energy and overlap in the three-point function are fit parameters. We will refer to this as *M2* fit.

We follow Ref. [19] and use the matrix element of the temporal component of the axial vector current, A_0, which is very precise, in order to determine the first excited energy and overlap. The temporal component has not been used in past studies, since it has been found to suffer from large excited state contributions. For more details see Ref. [25].

In Fig. 2 we show the energy of the first excited state extracted from fitting the two-point and the three-point function of A_0. We observe that the first excited energy extracted from the two-point function is in agreement with the energy of the Roper. We note that this is different from what is observed in two recent studies [19, 22], where the first excited state extracted from the two-point function is much higher. Moreover, the energy of the first excited state extracted from the three-point function, is in general in agreement with the energy of the non-interacting two-particle states of $N(0)+\pi(-\vec{p})$ and $N(\vec{p})+\pi(-\vec{p})$.

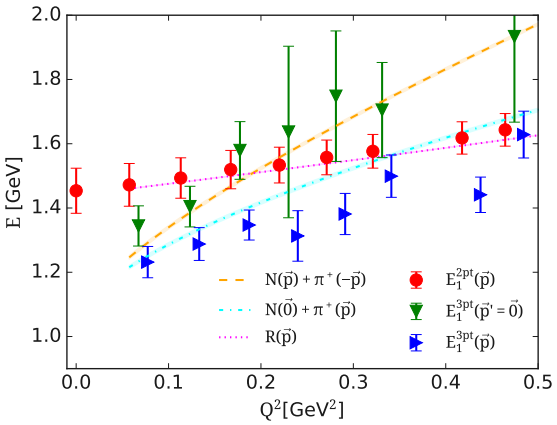

Figure 2: The energy of the first excited state as a function of Q^2. The orange dashed and cyan dashed-dotted lines are the energies of the non-interacting systems $N(\vec{p})+\pi(-\vec{p})$ and $N(\vec{0})+\pi(\vec{p})$, respectively, and the magenta dotted line is the Roper energy. The red circles are extracted by a two-state fit to the two-point function. The blue right- and green down-pointing triangles are $E_1^{3pt}(\vec{p})$ and $E_1^{3pt}(\vec{p}\,'=\vec{0})$ extracted from the three-point function of the temporal axial-vector current with a two-state fit. Figure is taken from Ref. [25].

4 Renormalization

The lattice QCD matrix elements need to be renormalized in order to extract physical form factors. A detailed description of our procedure can be found in Ref. [37]. In the twisted mass formulation and for the quantities of interest here, we need the renormalization functions Z_S for the renormalization of pseudoscalar current, Z_P for the renormalization of the bare quark mass and Z_A for the renormalization of the axial-vector current. Z_P and Z_S are scheme and scale dependent. Therefore, after the extrapolation $(am_\pi)^2 \to 0$, we convert to the $\overline{\text{MS}}$-scheme, which is commonly used in experimental and phenomenological studies. The conversion procedure is applied on the Z-factors at each initial RI′ scale ($a\,\mu_0$), with a simultaneous evolution to a $\overline{\text{MS}}$ scale, chosen to be $\overline{\mu}$=2 GeV. For the conversion and evolution we employ the intermediate Renormalization Group Invariant (RGI) scheme, which is scale independent.

5 Results on isovector form factors

Our main results are obtained using an ensemble simulated with two mass degenerate u- and d-quarks, a strange and a charm quark with mass tuned to approximately the physical one ($N_f = 2+1+1$), lattice spacing $a = 0.08$ fm and spatial lattice size $L = 5.12$ fm or $m_\pi L = 3.62$ with pion mass $m_\pi = 0.139(1)$ GeV, used as a proxy for finite volume effects. We refer to this ensemble as cB211.64. For isovector form factors only the connected contributions are needed.

In Fig. 3 we show results for the three form factors using the fit procedures *M1* and *M2* and compared with the pion-pole dominance relation of Eq. (8) for $G_P(Q^2)$ and combining Eq.(8) and the PCAC relation of Eq. (3) for $G_5(Q^2)$. We find that allowing the first excited state energy to be different in the two- and three-point functions has a negligible effect on G_A and a larger effect on G_P and G_5 but not large enough to fulfil the predicted behaviour from pion pole dominance

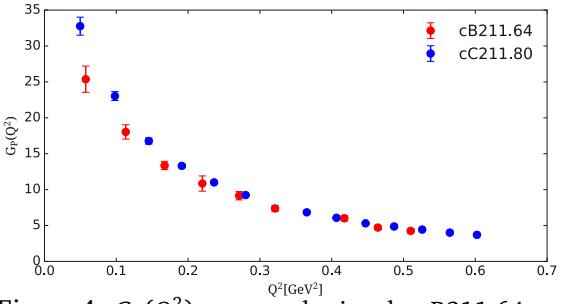

Figure 4: $G_P(Q^2)$ computed using the cB211.64 ensemble and an $N_f = 2+1+1$ ensemble (cC211.80) with $a = 0.07$ fm. Both ensembles have similar volume and $m_\pi = 0.139$ GeV. Figure taken from Ref. [25].

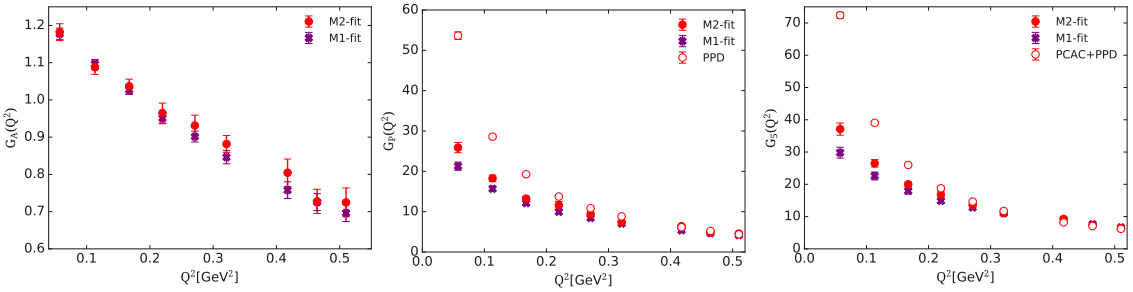

Figure 3: Results for the $G_A(Q^2)$ (left), $G_P(Q^2)$ (middle) and $G_5(Q^2)$ (right) form factors as a function of Q^2 from the analysis of the cB211.64 ensemble. Filled red circles are results using *M2* approach and purple crosses using *M1*. Open red circles are results using Eq.(8) for $G_P(Q^2)$ and combining Eq.(8) and Eq. (3) for $G_5(Q^2)$.

(PPD). As a consequence, the PCAC and PPD relations are not satisfied at low Q^2. Other lattice QCD collaborations find a bigger effect when not constraining the first excited state energy in the three-point function, resulting in satisfying the PPD relation [19, 38]. In order to understand the origin of the discrepancy in the PPD and PCAC relations, we examine lattice spacing effects by analysing an additional $N_f = 2+1+1$ ensemble with $a = 0.07$ fm and similar volume. Preliminary results, shown in Fig. 4, illustrate that G_P increases at low Q^2 as a decreases and so the continuum limit is important in recovering the PPD and PCAC relations. Since to take the continuum limit we need at least three lattice spacings, for the results that follow, we will use the PCAC and PPD relations to obtain G_P and G_5 from the lattice data on G_A. In Fig. 5

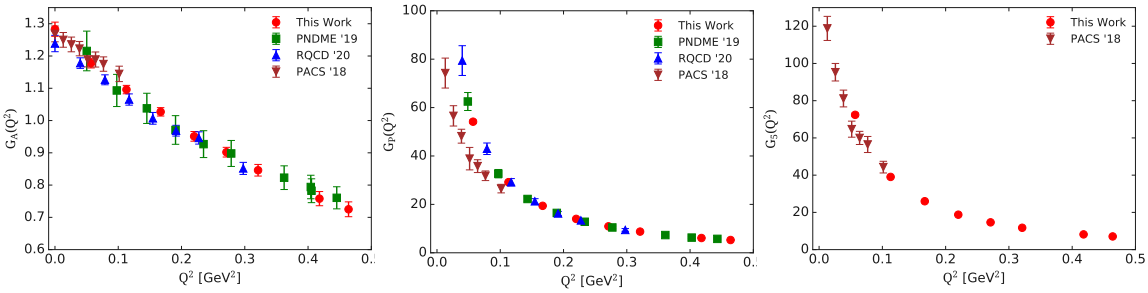

Figure 5: Lattice QCD results on the isovector axial $G_A(Q^2)$ (left), $G_P(Q^2)$ (middle) and $G_5(Q^2)$ using simulations with physical pion masses. Results using the cB211.64 ensemble are shown with red circles, from the PNDME collaboration [19] with green squares, from the RQCD collaboration [22] with blue upward-pointing triangles and from the PACS collaboration [23] with brown down-pointing triangles. Figure taken from Ref. [25].

we compare our results with those by other lattice QCD collaborations. Overall, there is a very good agreement among all results for $G_A(Q^2)$. PACS results [23] are available for very small Q^2 values since their lattice spatial extent is approximately twice as compared to the size of the other lattices. Furthermore, unlike other lattice QCD results shown, PACS extracted the results using the plateau method at the largest time separation available. The results from the PNDME and RQCD collaborations were extracted using the type-*M2* fit. Our results for $G_P(Q^2)$ are determined from $G_A(Q^2)$ and Eq. (3) and are in agreement with the results of PNDME and RQCD that were extracted directly form the matrix element without using $G_A(Q^2)$. Results on $G_P(Q^2)$ from PACS are lower at small Q^2 values, but their $G_P(Q^2)$ has been determined using the plateau fits at relatively small value of the source-sink separations. Our data on $G_5(Q^2)$ also used $G_A(Q^2)$ and PPD and agree with those from PACS computed directly form the matrix element of the pseudoscalar operator.

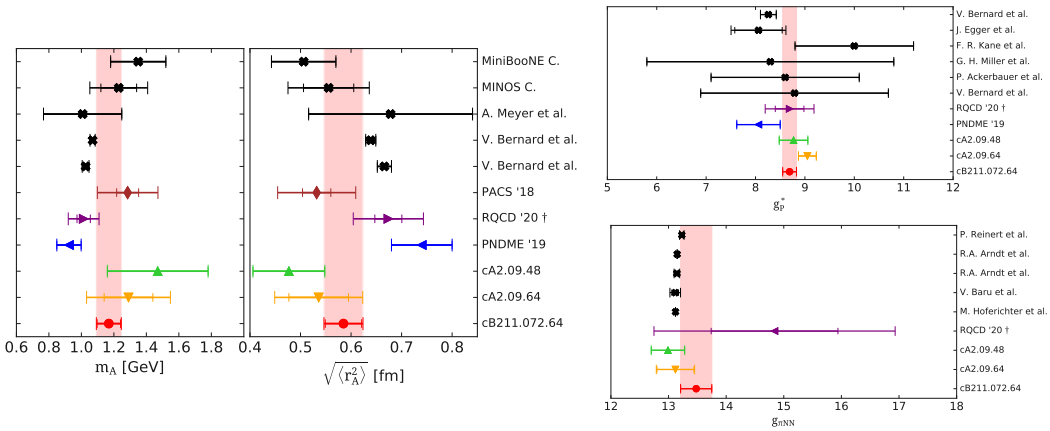

Figure 6: Left panel: Results on the isovector axial mass m_A (left) and the axial radius $\sqrt{\langle r_A^2 \rangle}$ (right). Right panel: Results for the muon capture coupling constant, g_P^* (top) and the pion-nucleon coupling $g_{\pi NN}$ (bottom). Red circles with the associated red band are the results using the cB211.64 ensemble. Results re also shown for two $N_f = 2$ twisted mass fermion ensembles with $a = 0.094$ fm and $L = 4.5$ fm (green up triangle) and 6.0 fm (orange down triangle), for PNDME [19] (blue left-pointing triangle), for RQCD [22] (purple right-pointing triangle, with † are results obtained after chiral and continuum extrapolation), and for PACS [23] (brown rhombus). Inner error bars are statistical errors while outer errors bars include systematic errors. The black crosses are results from phenomenology. Figure taken from Ref. [25], modified by including the phenomenological value of $g_{\pi NN}$ from Ref. [39].

Results on the axial mass m_A and root mean square radius $\sqrt{\langle r_A^2 \rangle}$, the muon capture coupling constant, g_P^* and the pion-nucleon coupling $g_{\pi NN}$ are compared to those of other recent lattice QCD studies using physical point ensembles, experimental results and phenomenology in Fig. 6. Lattice QCD results are in agreement amongst them. Phenomenological results are in general much more precise for $g_{\pi NN}$. On the other hand, experimental results on g_P^* from ordinary muon capture are compatible with lattice QCD results but carry large errors, while the result from chiral perturbation theory [40], is as precise as our value from the analysis of the cB211.64 ensemble.

6 Flavor decomposition of axial form factors

In order to compute the isoscalar, strange and charm form factors, we need to include the disconnected three-point function, schematically shown in Fig. 1. An order of magnitude more computational resources are needed to calculate these contributions as compared to the connected ones. We also need to compute the non-singlet renormalization functions, see Ref. [26].

We show results for the isoscalar axial form factors $G_A^{u+d}(Q^2)$ and $G_P^{u+d}(Q^2)$ in Fig. 7. We observe that the connected contribution is positive, while the disconnected is negative. For $G_P^{u+d}(Q^2)$, the disconnected part is of the same magnitude as the connected. This has already been observed in previous studies [18, 41]. This behavior leads to the cancellation of the sharp rise observed in the connected only isoscalar $G_P^{u+d}(Q^2)$. Consequently, the isoscalar has an almost flat Q^2-dependence, unlike the isovector combination discussed in the Sec. 5. We use the dipole Ansatz and the z-expansion to fit the Q^2 dependence of $G_A^{u+d}(Q^2)$ shown in Fig. 7. We find $g_A^{u+d} = 0.436(28)$ in agreement with our previous study [42]. The results for the strange and charm axial form factors are shown in Fig. 8 and are clearly non-zero. $G_A^s(0)$ gives the strange axial charge and we find $g_A^s = -0.044(8)$, while for the charm axial charge we find $g_A^c = -0.0098(17)$. In the SU(3) limit disconnected contributions should vanish in the octet combination u+d-2s. Instead, we observe deviations of up to 10% for $G_A^{u+d-2s}(0)$ and up to 50% for $G_P^{u+d-2s}(0)$.

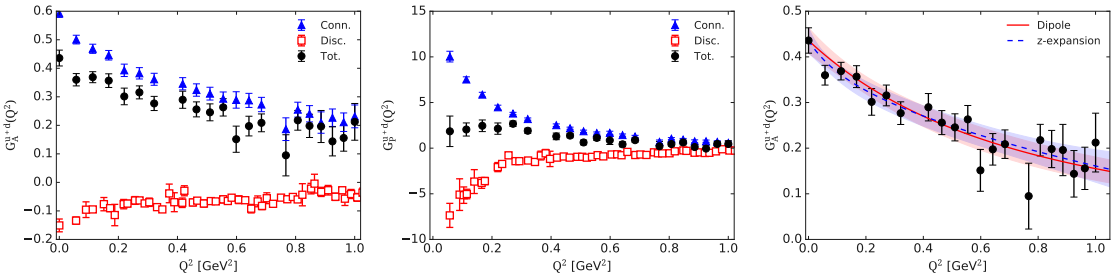

Figure 7: Renormalized results for the isoscalar $G_A^{u+d}(Q^2)$ (left) and $G_P^{u+d}(Q^2)$ (middle) as a function of Q^2. We show separately the connected (blue triangles) and the disconnected (open red squares) contributions as well as the sum (black circles). Open symbols are used for the form factors versus Q^2 when showing only disconnected contributions. Right: With the solid red line we show the dipole fit and the dashed blue of the z-expansion fit to $G_A^{u+d}(Q^2)$. Figure taken from Ref. [26].

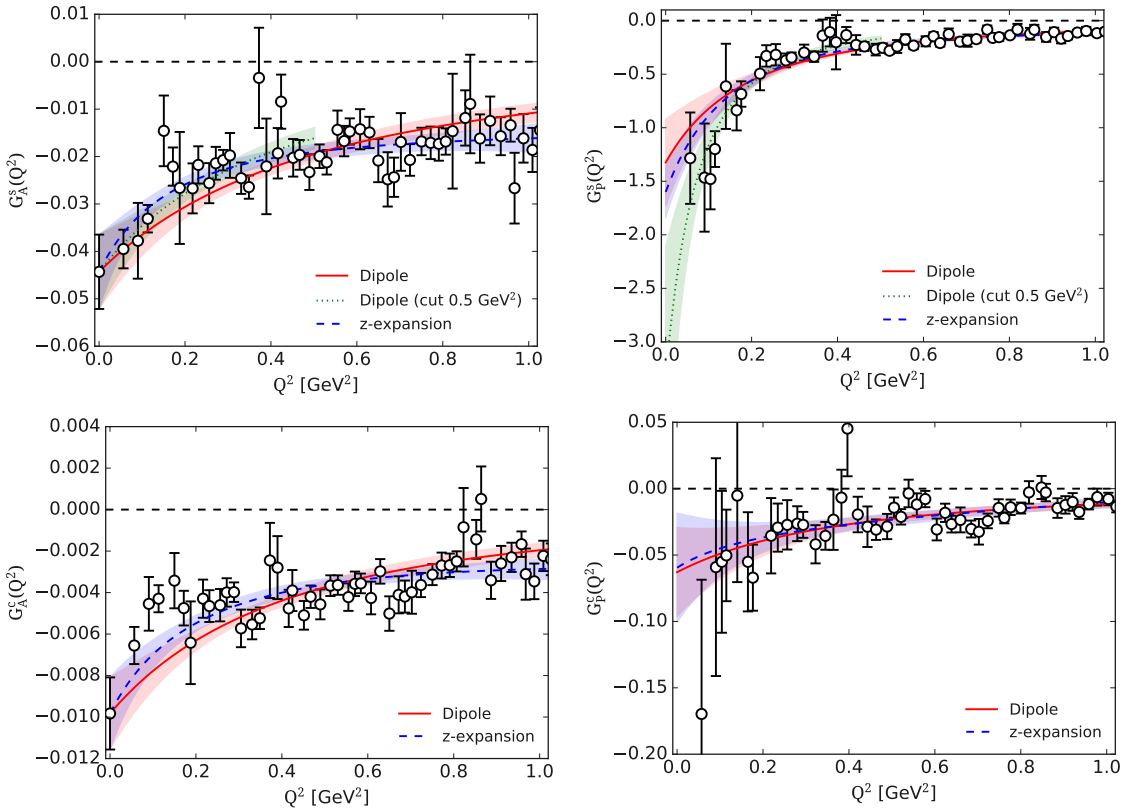

Figure 8: Left: Results for the strange $G_A^s(Q^2)$ (top) and charm $G_A^c(Q^2)$ (bottom) and right: result for the strange $G_P^s(Q^2)$ (top) and charm $G_P^C(Q^2)$ form factors as a function of Q^2. We show the fits using the dipole from and z-expansion as well as the dipole form fit taking the upper fit range up to ≃0.5 GeV^2 (green dotted line and band). Figure taken from Ref. [26].

7 Conclusions

Axial form factors including contributions from non-valence quarks can be extracted precisely enabling us to extract a lot of interesting physics and make predictions. The calculation of sea quark contributions is feasible providing valuable input e.g. for the determination of strange and charm form factors and for checking SU(3) symmetry. Further study of the PCAC and Goldberger-Treiman relations is required. In particular, taking the continuum limit will be a major next step.

Acknowledgements

We would like to thank all members of the Extended Twisted Mass Collaboration for a very constructive and enjoyable collaboration and in particular our close collaborators for this work S. Bacchio, M. Constantinou, P. Dimopoulos, J. Finkenrath, K. Hadjiyiannakou, K. Jansen, G. Koutsou, B. Kostrze, T. Leontiou and C. Urbach. This project has received funding from the Horizon 2020 research and innovation program of the European Commission under the Marie Skłodowska-Curie grant agreement No 642069(HPC-LEAP) and under grant agreement No 765048 (STIMULATE), by the H2020 project PRACE 6-IP (grant agreement No 82376) and by the Cyprus Research and Innovation foundation under contract number POST-DOC/0718/0100 and the COMPLEMENTARY/0916/0015 project. Computational resources were received by the Gauss Centre for Supercomputing e.V. (www.gauss-centre.eu) under project pr74yo run on SuperMUC at Leibniz Supercomputing Centre (www.lrz.de), Piz Daint at Centro Svizzero di Calcolo Scientifico, via the project with id s702, from the John von Neumann-Institute for Computing on the Jureca system [43] at the research center in Jülich, under the project with id ECY00 and HCH02, and from Extreme Science and Engineering Discovery Environment (XSEDE), which is supported by National Science Foundation grant number TG-PHY170022.

References

[1] X. Yan *et al.*, *Robust extraction of the proton charge radius from electron-proton scattering data*, Phys. Rev. C **98**(2), 025204 (2018), doi:10.1103/PhysRevC.98.025204, 1803.01629.

[2] M. Ablikim *et al.*, *Measurement of proton electromagnetic form factors in $e^+e^- \to p\bar{p}$ in the energy region 2.00 - 3.08 GeV*, Phys. Rev. Lett. **124**(4), 042001 (2020), doi:10.1103/PhysRevLett.124.042001, 1905.09001.

[3] L. Ahrens *et al.*, *A Study of the Axial Vector Form-factor and Second Class Currents in Anti-neutrino Quasielastic Scattering*, Phys. Lett. B **202**, 284 (1988), doi:10.1016/0370-2693(88)90026-3.

[4] A. S. Meyer, M. Betancourt, R. Gran and R. J. Hill, *Deuterium target data for precision neutrino-nucleus cross sections*, Phys. Rev. **D93**(11), 113015 (2016), doi:10.1103/PhysRevD.93.113015, 1603.03048.

[5] S. Choi *et al.*, *Axial and pseudoscalar nucleon form-factors from low-energy pion electroproduction*, Phys. Rev. Lett. **71**, 3927 (1993), doi:10.1103/PhysRevLett.71.3927.

[6] M.-P. Brown *et al.*, *New result for the neutron β-asymmetry parameter A_0 from UCNA*, Phys. Rev. C **97**(3), 035505 (2018), doi:10.1103/PhysRevC.97.035505, 1712.00884.

[7] D. Mund *et al.*, *Determination of the Weak Axial Vector Coupling from a Measurement of the Beta-Asymmetry Parameter A in Neutron Beta Decay*, Phys. Rev. Lett. **110**, 172502 (2013), doi:10.1103/PhysRevLett.110.172502, 1204.0013.

[8] J. Castro and C. Dominguez, *Upper Bound for the Induced Pseudoscalar Form-Factor in Muon Capture*, Phys. Rev. Lett. **39**, 440 (1977), doi:10.1103/PhysRevLett.39.440.

[9] V. Andreev *et al.*, *Measurement of the rate of muon capture in hydrogen gas and determination of the proton's pseudoscalar coupling g(P)*, Phys. Rev. Lett. **99**, 032002 (2007), doi:10.1103/PhysRevLett.99.032002, 0704.2072.

[10] K. A. Aniol *et al.*, *Parity violating electroweak asymmetry in polarized-e p scattering*, Phys. Rev. C **69**, 065501 (2004), doi:10.1103/PhysRevC.69.065501, nucl-ex/0402004.

[11] L. A. Ahrens *et al.*, *Measurement of Neutrino - Proton and anti-neutrino - Proton Elastic Scattering*, Phys. Rev. D **35**, 785 (1987), doi:10.1103/PhysRevD.35.785.

[12] S. F. Pate, *Determination of the strange form-factors of the nucleon from nu p, anti-nu p, and parity violating polarized-e p elastic scattering*, Phys. Rev. Lett. **92**, 082002 (2004), doi:10.1103/PhysRevLett.92.082002, hep-ex/0310052.

[13] D. S. Armstrong *et al.*, *Strange quark contributions to parity-violating asymmetries in the forward G0 electron-proton scattering experiment*, Phys. Rev. Lett. **95**, 092001 (2005), doi:10.1103/PhysRevLett.95.092001, nucl-ex/0506021.

[14] D. Androic *et al.*, *Strange Quark Contributions to Parity-Violating Asymmetries in the Backward Angle G0 Electron Scattering Experiment*, Phys. Rev. Lett. **104**, 012001 (2010), doi:10.1103/PhysRevLett.104.012001, 0909.5107.

[15] B. Abi *et al.*, *Long-baseline neutrino oscillation physics potential of the DUNE experiment*, Eur. Phys. J. C **80**(10), 978 (2020), doi:10.1140/epjc/s10052-020-08456-z, 2006.16043.

[16] K. Abe *et al.*, *The Hyper-Kamiokande Experiment - Snowmass LOI*, In *2022 Snowmass Summer Study* (2020), 2009.00794.

[17] C. Alexandrou, G. Koutsou, T. Leontiou, J. W. Negele and A. Tsapalis, *Axial Nucleon and Nucleon to Delta form factors and the Goldberger-Treiman Relations from Lattice QCD*, Phys. Rev. D **76**, 094511 (2007), doi:10.1103/PhysRevD.80.099901, [Erratum: Phys.Rev.D 80, 099901 (2009)], 0706.3011.

[18] C. Alexandrou *et al.*, *Nucleon axial form factors using $N_f = 2$ twisted mass fermions with a physical value of the pion mass*, Phys. Rev. D **96**(5), 054507 (2017), doi:10.1103/PhysRevD.96.054507, 1705.03399.

[19] Y.-C. Jang, R. Gupta, B. Yoon and T. Bhattacharya, *Axial Vector Form Factors from Lattice QCD that Satisfy the PCAC Relation*, Phys. Rev. Lett. **124**(7), 072002 (2020), doi:10.1103/PhysRevLett.124.072002, 1905.06470.

[20] R. Gupta, Y.-C. Jang, H.-W. Lin, B. Yoon and T. Bhattacharya, *Axial Vector Form Factors of the Nucleon from Lattice QCD*, Phys. Rev. D **96**(11), 114503 (2017), doi:10.1103/PhysRevD.96.114503, 1705.06834.

[21] G. Bali, S. Collins, M. Gruber, A. Schäfer, P. Wein and T. Wurm, *Solving the PCAC puzzle for nucleon axial and pseudoscalar form factors*, Phys. Lett. B **789**, 666 (2019), doi:10.1016/j.physletb.2018.12.053, 1810.05569.

[22] G. S. Bali *et al.*, *Nucleon axial structure from lattice QCD*, JHEP **05**, 126 (2020), doi:10.1007/JHEP05(2020)126, 1911.13150.

[23] E. Shintani, K.-I. Ishikawa, Y. Kuramashi, S. Sasaki and T. Yamazaki, *Nucleon form factors and root-mean-square radii on a (10.8 fm)^4 lattice at the physical point*, Phys. Rev. D **99**(1), 014510 (2019), doi:10.1103/PhysRevD.99.014510, 1811.07292.

[24] K.-I. Ishikawa, Y. Kuramashi, S. Sasaki, N. Tsukamoto, A. Ukawa and T. Yamazaki, *Nucleon form factors on a large volume lattice near the physical point in 2+1 flavor QCD*, Phys. Rev. D **98**(7), 074510 (2018), doi:10.1103/PhysRevD.98.074510, 1807.03974.

[25] C. Alexandrou *et al.*, *Nucleon axial and pseudoscalar form factors from lattice QCD at the physical point*, Phys. Rev. D **103**(3), 034509 (2021), doi:10.1103/PhysRevD.103.034509, 2011.13342.

[26] C. Alexandrou, S. Bacchio, M. Constantinou, K. Hadjiyiannakou, K. Jansen and G. Koutsou, *Quark flavor decomposition of the nucleon axial form factors*, Phys. Rev. D **104**, 074503 (2021), doi:10.1103/PhysRevD.104.074503, 2106.13468.

[27] C. Alexandrou, G. Koutsou, T. Leontiou, J. W. Negele and A. Tsapalis, *Nucleon and nucleon to Delta axial form-factors from lattice QCD*, PoS **LATTICE2007**, 162 (2007), doi:10.22323/1.042.0162, 0710.2173.

[28] M. Goldberger and S. Treiman, *Form-factors in Beta decay and muon capture*, Phys. Rev. **111**, 354 (1958), doi:10.1103/PhysRev.111.354.

[29] M. Scadron, *Advanced quantum theory and its applications through Feynman diagrams* (1991).

[30] M. Nagy and M. D. Scadron, *Pion nucleon coupling constant, Goldberger-Treiman discrepancy and pi N sigma term*, Acta Phys. Slov. **54**, 427 (2003), hep-ph/0406009.

[31] C. Alexandrou, M. Constantinou, S. Dinter, V. Drach, K. Jansen, C. Kallidonis and G. Koutsou, *Nucleon form factors and moments of generalized parton distributions using $N_f = 2+1+1$ twisted mass fermions*, Phys. Rev. **D88**(1), 014509 (2013), doi:10.1103/PhysRevD.88.014509, 1303.5979.

[32] C. Alexandrou, M. Brinet, J. Carbonell, M. Constantinou, P. A. Harraud, P. Guichon, K. Jansen, T. Korzec and M. Papinutto, *Nucleon electromagnetic form factors in twisted mass lattice QCD*, Phys. Rev. **D83**, 094502 (2011), doi:10.1103/PhysRevD.83.094502, 1102.2208.

[33] C. Alexandrou, G. Koutsou, J. W. Negele and A. Tsapalis, *The Nucleon electromagnetic form factors from Lattice QCD*, Phys. Rev. **D74**, 034508 (2006), doi:10.1103/PhysRevD.74.034508, hep-lat/0605017.

[34] P. Hagler, J. W. Negele, D. B. Renner, W. Schroers, T. Lippert and K. Schilling, *Moments of nucleon generalized parton distributions in lattice QCD*, Phys. Rev. **D68**, 034505 (2003), doi:10.1103/PhysRevD.68.034505, hep-lat/0304018.

[35] O. Bar, *$N\pi$-state contamination in lattice calculations of the nucleon axial form factors*, Phys. Rev. D **99**(5), 054506 (2019), doi:10.1103/PhysRevD.99.054506, 1812.09191.

[36] O. Bar, *$N\pi$-excited state contamination in nucleon 3-point functions using ChPT*, In *37th International Symposium on Lattice Field Theory* (2019), 1907.03284.

[37] C. Alexandrou, M. Constantinou and H. Panagopoulos, *Renormalization functions for Nf=2 and Nf=4 twisted mass fermions*, Phys. Rev. D **95**(3), 034505 (2017), doi:10.1103/PhysRevD.95.034505, 1509.00213.

[38] G. S. Bali, L. Barca, S. Collins, M. Gruber, M. Löffler, A. Schäfer, W. Söldner, P. Wein, S. Weishäupl and T. Wurm, *Nucleon axial structure from lattice QCD*, JHEP **05**, 126 (2020), doi:10.1007/JHEP05(2020)126, 1911.13150.

[39] P. Reinert, H. Krebs and E. Epelbaum, *Precision determination of pion-nucleon coupling constants using effective field theory*, Phys. Rev. Lett. **126**(9), 092501 (2021), doi:10.1103/PhysRevLett.126.092501, 2006.15360.

[40] V. Bernard, L. Elouadrhiri and U.-G. Meissner, *Axial structure of the nucleon: Topical Review*, J. Phys. G **28**, R1 (2002), doi:10.1088/0954-3899/28/1/201, hep-ph/0107088.

[41] J. Green, N. Hasan, S. Meinel, M. Engelhardt, S. Krieg, J. Laeuchli, J. Negele, K. Orginos, A. Pochinsky and S. Syritsyn, *Up, down, and strange nucleon axial form factors from lattice QCD*, Phys. Rev. D **95**(11), 114502 (2017), doi:10.1103/PhysRevD.95.114502, 1703.06703.

[42] C. Alexandrou, S. Bacchio, M. Constantinou, J. Finkenrath, K. Hadjiyiannakou, K. Jansen, G. Koutsou and A. Vaquero Aviles-Casco, *The nucleon axial, tensor and scalar charges and σ-terms in lattice QCD* (2019), 1909.00485.

[43] Jülich Supercomputing Centre, *JURECA: Modular supercomputer at Jülich Supercomputing Centre*, Journal of large-scale research facilities **4**(A132) (2018), doi:10.17815/jlsrf-4-121-1.